DOI: 10.1002/ejic.200600641

Facile Synthesis of Oligothiophene-Capped CdS Nanoparticles

Tarek Antoun,[a] Roberta Brayner,[a] Seham Al terary,[a] Fernand Fiévet,[a] Mohamed Chehimi,[a] and Abderrahim Yassar*[a]

Keywords: Nanoparticle synthesis / Oligothiophenes / Photovoltaics / Conjugated polymers / Nanostructures

CdS nanoparticles functionalized by electroactive oligothiophenes, with narrow size distribution, have been prepared and characterized. The structure of the hybrid product was investigated by TEM, XRD, optical and FTIR spectroscopy. The modified nanoparticles consist of a few tens of oligothiophene units attached to the CdS core. The grafting of conjugated oligomers to nanoparticles was made possible by complexing the dangling cadmium ion on the nanoparticle surface.

Introduction

The design of nanostructured hybrid materials, with novel physical properties, has emerged as one of the most exciting areas of scientific endeavour in this decade, in which material and chemical research are playing a dominant role.[1] Nanocrystals (NCs) have a well-documented array of properties that differ from those of the corresponding bulk materials. Surface modification was shown to optimize the intrinsic optical properties, producing highly luminescent NCs, and also serves as a means of tuning their solubility. On the other hand, π-conjugated oligomers and polymers are a relatively new class of electronic materials that are revolutionizing important technological applications including large-area electronics, owing to their compatibility with low-temperature processing, the simplicity of thin-film device fabrication and the tunability of their electronic properties.[2] The richness of the synthetic organic chemistry allows the fabrication of π-conjugated materials with a degree of control unattainable with conventional inorganic semiconductors. Grafting conjugated polymers and oligomers onto the surface of nanoparticles provides a means of controlling not only the final surface functionality of the material, as one could do also with ligands, but also of introducing new optoelectronic and enhancing charge-transport properties.[3] Such physical properties have motivated many studies on π-conjugated systems and NC composites.

The encapsulation of inorganic nanoparticles by conjugated polymers has its origin in work by Greenham et al. which dates back over one decade.[4] Although much attention has been devoted to the study of the photovoltaic properties of these materials, there have been studies reporting the elaboration and the characterization of well-organized NCs embedded in conjugated polymers, as can be seen from reports of the Lahav group who studied the organization of $(Pb_{1-x}Cd_x)S$ nanoparticles within an oligo(*p*-phenyleneethylene)dicarboxylate matrix.[5] In optoelectronic devices, inorganic semiconductor NCs have been combined with π-conjugated systems in order to take advantage of the ease of processing, characteristic of many π-conjugated polymers, and their complementary properties. The inorganic semiconductor NCs have high electron affinities and the organic semiconductors show high hole mobilities, so charge transfer occurs rapidly in such systems. Photoinduced charge transfer can result in enhancement of the photoconductivity and photovoltaic effects. A major problem which arises in the fabrication of these composites is the immiscibility of the two materials due to differences in their polarities. In composites heavily loaded with NCs, phase segregation occurs even when the NCs are stabilized by hydrophilic ligands.[4]

To overcome this problem and to obtain a three-dimensional interpenetrating network of nanocomposites, many approaches have been used, in which NCs and conjugated polymers are intimately associated. In these approaches the conjugated systems are directly connected to the quantum dot surface. Milliron et al. reported the preparation of novel soluble oligothiophene-CdSe NCs, wherein electronic interaction between functional components was facilitated by attaching the binding group directly to the conjugated backbone.[6] Mutual fluorescence quenching of oligothiophenes and CdSe NCs indicates photoinduced charge transfer, which is essential for their potential utility as an active component in photovoltaic devices. Similarly, Sun et al. have

[a] Interfaces, Traitements, Organisation et Dynamique des Systèmes, CNRS, UMR 7086, Université Diderot (Paris 7), 1 rue Guy de la Brosse, 75005 Paris, France

demonstrated that devices fabricated from blends of tetrapod CdSe nanoparticles and a conjugated polymer perform better than devices made from nanorod/polymer blends.[7] The authors believe that the control of the NC shape provides an additional tool to control morphology and facilitate the charge transfer process. Nanocomposites based on TiO_2 nanoparticles functionalized by conjugated terthiophenecarboxylic acid have been prepared and characterized by Beek et al.[8] The fluorescence of the terthiophene moiety was completely quenched due to photoinduced electron transfer from terthiophene to titanium dioxide. The quenching is believed to be predominantly static rather than dynamic.

The role of organic surfactants and morphology control have been pointed out by Liu et al.[9] In their work, they showed that an end-functional poly(3-hexylthiophene) (P3HT) enhances the performance of P3HT/CdSe nanocrystal solar cells by increasing the dispersion of CdSe without introducing insulating surfactants. Despite several reports of various NC post-functionalization procedures, much development is still needed to elaborate NC-π-conjugated systems, in which the two components are in intimate contact and electron transfer is not altered by the presence of insulating surfactants. On the basis of a survey of published accounts, CdSe and CdS quantum dots are II–VI semiconductor nanoparticles. There is no distinction that separates the two nanoparticles in terms of desirable properties for applications. CdSe nanoparticles and π-conjugated polymers have to date been the most-studied nanocomposite materials; however, one of the limitations of CdSe nanoparticle synthesis is the use of hazardous and pyrophoric compounds such as dimethylcadmium, $(CH_3)_2CdSe$, TOPO and, especially, the high temperatures (300 °C) that are required. In contrast the synthesis of CdS is safer. These reasons motivated our choice of CdS nanoparticles as models to develop a versatile one-pot method for preparing CdS NC-bound conjugated materials.

In this work we report a one-pot method for preparing CdS NC-bound oligothiophenes. Transmission electron microscopy (TEM) and X-ray diffraction powder (XRD) show that the CdS nanoparticles are monodisperse. The amount of oligothiophene and the nature of surface binding are studied in detail using X-ray photoelectron spectroscopy (XPS), IR, UV/Vis and fluorescence spectroscopy. The major advantage of this method is that we use functionalized π-conjugated electroactive systems as ligands to control NC growth. The electroactive ligand binds to the NC surface, and allows intimate contact between the NC and the conjugated oligomer backbone leading to better electronic communication between the two components. The bonding of the oligomers to the NC surface was made possible by complexing the dangling cadmium ion on the NC surface by the lone-pair electrons of the carboxylate group in the oligomer. We have also found the carboxylate function to be a versatile and stable ligating group that can be easily attached to II–VI semiconductor nanoparticle surfaces.

Results and Discussion

Scheme 1 depicts the chemical structures of the α,ω-oligothiophene dicarboxylic acids used in this study. 2,2′-Bithiophene-5,5′-dicarboxylic acid (**I**), 2,2′;5′,2′′-terthiophene-5,5′′-dicarboxylic acid (**II**), and 2,2′;5′,2′′;5′′,2′′′-quaterthiophene-5,5′′′-dicarboxylic acid (**III**) were prepared as described in detail elsewhere.[10] CdS NCs capped with **I**, **II** and **III** (**CdS-2T**, **CdS-3T**, **CdS-4T**, respectively) were then prepared in ethylene glycol (EG) according to the polyol process;[11] see Scheme 2.

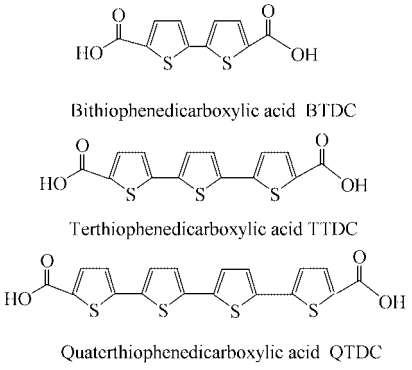

Scheme 1. Oligothiophenes used for the functionalization of CdS nanocrystals.

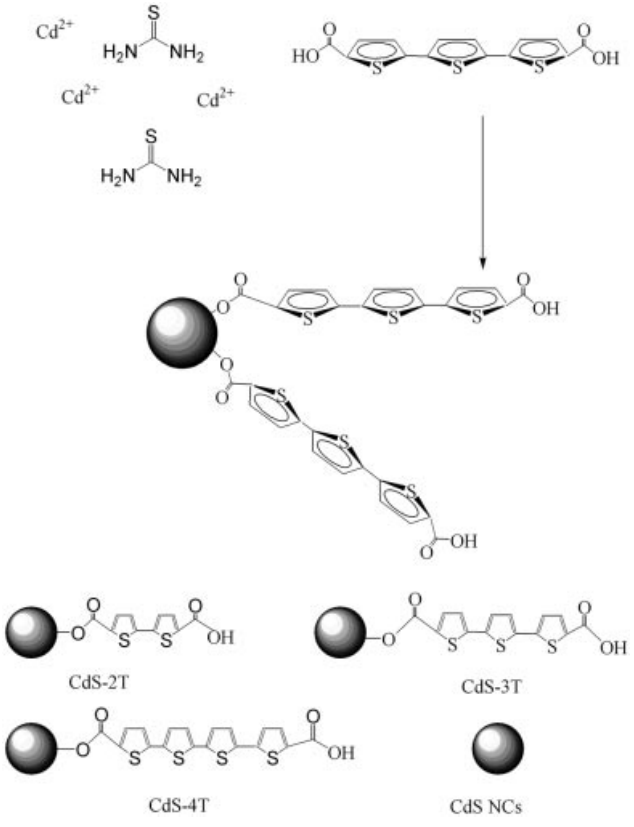

Scheme 2. Schematic representation of the preparation of CdS–oligothiophene by a one-pot procedure.

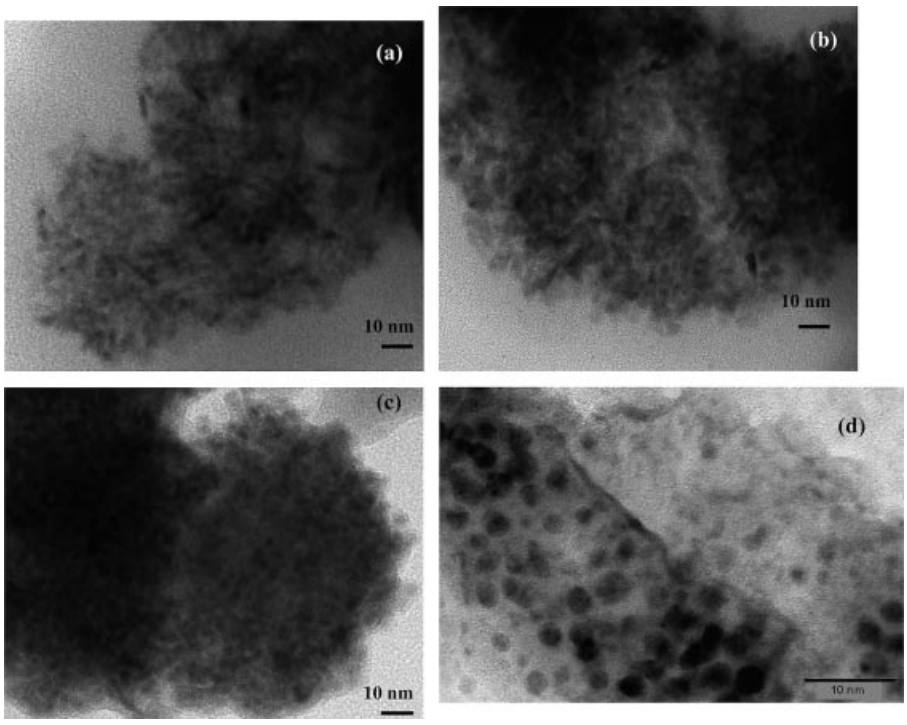

Figure 1. TEM micrographs of CdS–oligothiophene nanoparticles (a) **CdS-2T**; (b) **CdS-3T**; (c) **CdS-4T**; (d) **CdS-3T** prepared at pH = 9. The scale bar represents 10 nm in each case.

The general procedure involves addition of cadmium acetate and thiourea to a given volume of EG to obtain a concentration between 10^{-2} and 10^{-3} mol L^{-1}. To form CdS–oligothiophene hybrids, oligothiophenes were added to the reaction mixture in EG. The mixture was then heated with vigorous stirring to a temperature between 100 and 150 °C.

Transmission electron microscopy reveals that the oligothiophene molecules act as mediator templates towards the preparation of size-controlled spherical assemblies (50–200 nm) (Figure 1). The average individual CdS particle sizes are on the nanometer scale, 2–4 nm, depending on the conjugation length of the organic chain. In deionized water at pH = 9 CdS–oligothiophene nanoparticles are generally isolated from one another (Figure 1d). The assembly of CdS nanoparticles into nanospheres is believed to be a result of π–π interactions between conjugated systems.[12] The crystallinity of the **CdS-*n*T** samples was investigated by X-ray diffraction, as shown in Figure 2. At equilibrium reaction conditions, CdS nanoparticles present the thermodynamically stable hexagonal (wurtzite) structure. In this work, all samples can be indexed as cubic (sphalerite) in structure, showing (111), (220) and (311) peaks. This behaviour is perhaps due to the presence of oligothiophene molecules on the CdS surface. The same phase was observed by McPherson et al. for CdS synthesized in water-in-oil microemulsions using a combination of bis(2-ethylhexyl) sulfosuccinate (AOT) and the zwitterionic phospholipid L-α-phosphatidylcholine (lecithin).[13] An average size was estimated by applying Scherrer's formula. Crystallite sizes decrease with an increase in the conjugation length of the organic molecule, from 4 nm for **CdS-2T** to 2 nm for **CdS-4T**.

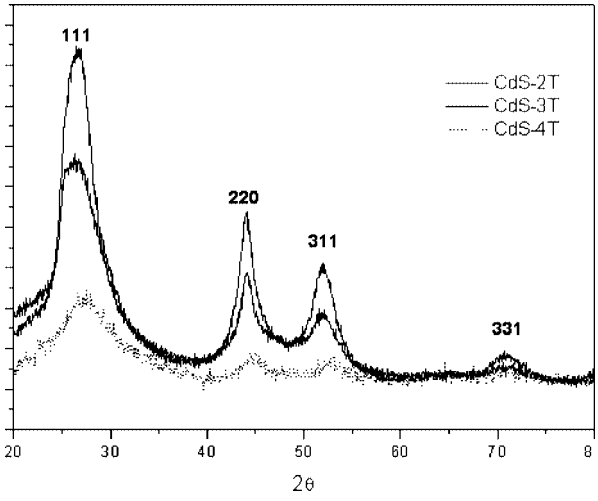

Figure 2. Powder X-ray diffraction patterns of three samples of **CdS-*n*T** nanoparticles.

The reduction of particle size with an increase in the conjugation length of the adsorbate can be understood as a passivation effect on the NC surface with longer oligomers. This result is somewhat surprising, that the steric effects are similar for the three oligomers, assuming they lie perpendicular to the NC surface. The HOMO–LUMO energy and carboxylate reactivity is an alternative explanation. In general, the smaller the HOMO–LUMO energy gap of an aromatic acid, the softer the anions. A soft base with smaller HOMO–LUMO energy will adsorb more readily on a surface. DFT calculations on the oligothiophenecarboxylates

show that changing the carboxylate from thiophene to bithiophene or terthiophene reduces the energy gap considerably.[14] The HOMO rises and the LUMO falls. In the light of these facts, we assume that the longer oligomers, i.e. **QTDC** and **TTDC** bind more strongly to the NC surface than **BTDC**; therefore, the longer oligomer straightforwardly passivates the NC surface and stops particle growth at an early stage of growth resulting in small nanoparticles.

FTIR spectroscopy was used to study CdS–oligothiophene core-shell structures and to reveal also the bonding mode of the organic molecule adsorbed on the NC. In the frequency region where C=C, C–C and C–S stretching vibrations are active, the infrared spectra of α,ω-oligothiophene diacids and **CdS-*n*T** show many similarities. These spectra exhibit characteristic bands of oligothiophenes that are centred at 1520, 1436, 890, 812 cm^{-1}, and 750 cm^{-1}, assigned to antisymmetric C=C, symmetric C=C, antisymmetric C–S, symmetric C–S stretching modes, and out-of-plane C–H deformation, respectively. However, we observe a slight vibration shift of the π-conjugated system upon adsorption of the oligomer on the NC surface. The ν_{ant} (C–C) and symmetric C–S modes are redshifted by 7 and 13 cm^{-1}, respectively. The out-of-plane deformation of C–H is blueshifted by 17 cm^{-1}. The change in the thiophene vibration can be attributed to the new electronic distribution of the bonded oligomers. Figure 3a, b represents typical FTIR spectra of the carboxylate region, for **BTDC**, **CdS-2T**, **TTDC** and **CdS-3T**.

The stretching band of the carbonyl group C=O, which appears at 1669 cm^{-1} for **BTDC** and 1663 cm^{-1} for **TTDC**, is no longer identified in the IR spectra of **CdS-*n*T**. Instead, the symmetric and asymmetric stretching vibrations of the COO^- group appear distinctly at 1386 and 1560 cm^{-1}, respectively. The shoulder at 1617 cm^{-1}, observed for **CdS-2T** indicates the existence of a second coordination mode of the carboxylate group. The intensity of the latter increases and becomes a distinct band for **CdS-3T**. The presence of the $\nu_s(COO^-)$ band in the **CdS-*n*T** spectra clearly indicates that the oligothiophene binds to the CdS surface through the carboxylate group. Also, observing two types of carboxylate stretches indicates that the carboxylate group of the oligomers function in different coordination fashions, two at least. The binding mode can be determined from the carboxylate band splitting. Hence, it was established that the mode of carboxylic acid coordination in complexes or adsorbed on a surface can be determined using infrared spectroscopy. There are four common carboxylate coordination modes: monodentate, chelating bidentate, bridging bidentate and ionic interaction. The coordination mode can be distinguished by the different separations between the antisymmetric and symmetric stretching adsorption bands ($\Delta\nu$).[15] Bidentate coordination modes of the carboxylate group show a separation less than 200 cm^{-1}, whereas monodentate modes show a larger separation. In the present work band separations of $\Delta\nu$ = 180 and 240 cm^{-1} were obtained for **CdS-3T**, indicating bidentate and monodentate coordination modes. The similarity of the **CdS-2T** spectrum and its band separations, $\Delta\nu$ = 180 and 230 cm^{-1}, indicates

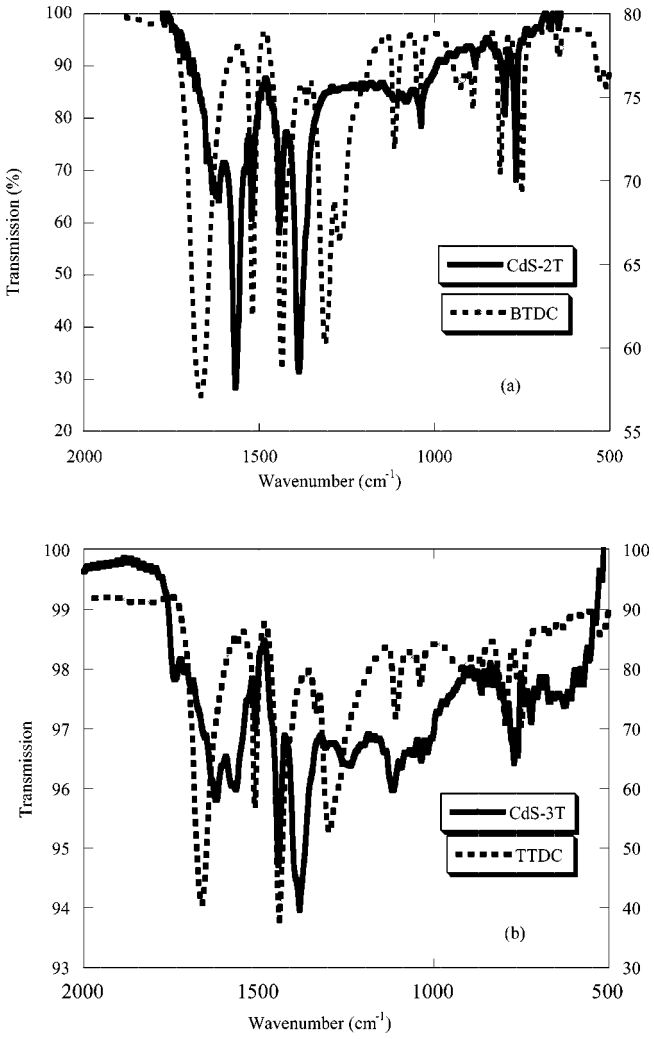

Figure 3. FT-IR spectra of (a) **BTDC** and **CdS-2T**, (b) **TTDC** and **CdS-3T**.

that a similar mode of binding occurs. The FTIR data show clearly that the final composition of the **CdS-*n*T** core shell includes both a thiophene oligomer shell and a CdS core. On the other hand, the complexation of oligothiophenecarboxylate with CdS nanoparticles occurs through strong ionic/covalent bonds. Also, the bonding of the oligomer on the NC surface deeply influences the electronic distribution of the π-conjugated system.

The elemental composition of the CdS–oligothiophene nanoparticles was analyzed by XPS. The XPS survey scan of **CdS-4T** is depicted in Figure 4, as a representative example. The main features, S2p, C1s, $Cd3d_{5/2}$ and O1s, are centred at 162, 285, 405 and 532 eV, respectively. The O1s/$Cd3d_{5/2}$ and C1s/$Cd3d_{5/2}$ intensity ratios differ markedly depending on the chemical structure of the oligomer, i.e. chain length. The high-resolution Cd3d region from **CdS-4T**, shown as an insert in Figure 4, exhibits $Cd3d_{5/2}$ and $Cd3d_{3/2}$ peaks (spin-orbit doublet) centred at 405.8 and 412.4 eV, respectively.

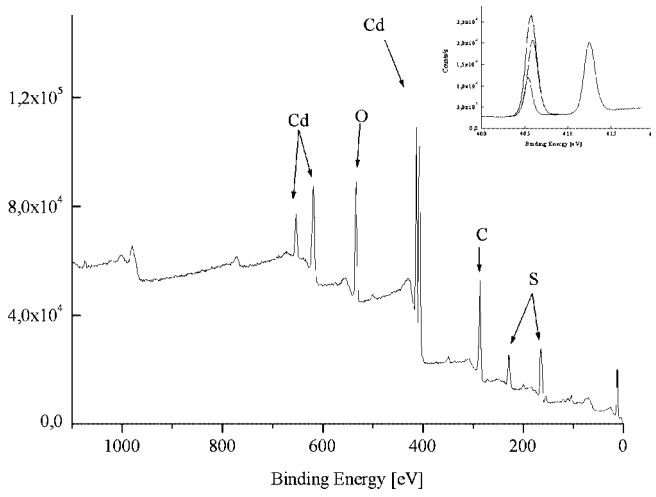

Figure 4. XPS survey scan of **CdS-4T**; the insert shows core level of $Cd3d_{5/2}$.

The $Cd3d_{5/2}$ binding energy is in line with the published data for CdS.[16] When care was taken to closely analyze the $Cd3d_{5/2}$ spectra, they were fitted with two peaks using Gaussian line shapes, which can be assigned to the bulk of Cd atoms, the second one at high binding energy, which should be attributed to surface cadmium atoms complexed to the oligomer through the carboxylate group. The surface contribution is about 20% of the total signal for **CdS-4T** and drops to 10% for **CdS-2T**. This is expected and is in agreement with literature data, which show that the surface contribution is larger for smaller NCs; the sizes of the nanoparticles are 4 and 2 nm for **CdS-2T** and **CdS-4T**, respectively.

Figure 5 compares the S2p regions of **CdS-2T** and **CdS-4T**. The spectra are fitted with three different spin-orbit split S2p doublets. The spin-orbit energy shift (ca. 1.2 eV) and the intensity ratio of 2:1 for the $S2p_{3/2}/S2p_{1/2}$ components has been taken to fit. The S2p peak-fitting parameters are reported in Table 1 for the three samples analyzed. The three components identified are attributed to sulfur in the bulk of CdS (161.9 eV), sulfur atoms from the oligothiophene (164.1 eV), the organic stabilizer bound to the nanoparticle, and a very small amount of oxidized sulfur (168.4 eV), from the oxidation of the particle surface. Table 2 reports the surface chemical composition (in percent) of the nanoparticles. Similarly, as previously observed for CdS and CdSe nanocrystals, the Cd^{2+}/S^{2-} atomic ratio is nonstoichiometric,[17] showing a significant excess of cadmium atoms on the surface, with the atomic ratio of Cd/S = 1.54, 1.52 and 1.43 for **CdS-2T**, **CdS-3T** and **CdS-4T**, respectively. It is reasonable to assume that the lack of sulfur in the outermost layers of the nanoparticles is compensated by the carboxylate groups from the oligothiophene capping ligands.

The production of highly monodisperse semiconductor nanocrystals requires stabilizers such as amines, phosphanes, phosphane oxides and phosphonic acids as capping ligands. However, a few recent reports have examined in detail the binding of long-chain carboxylic capping ligands

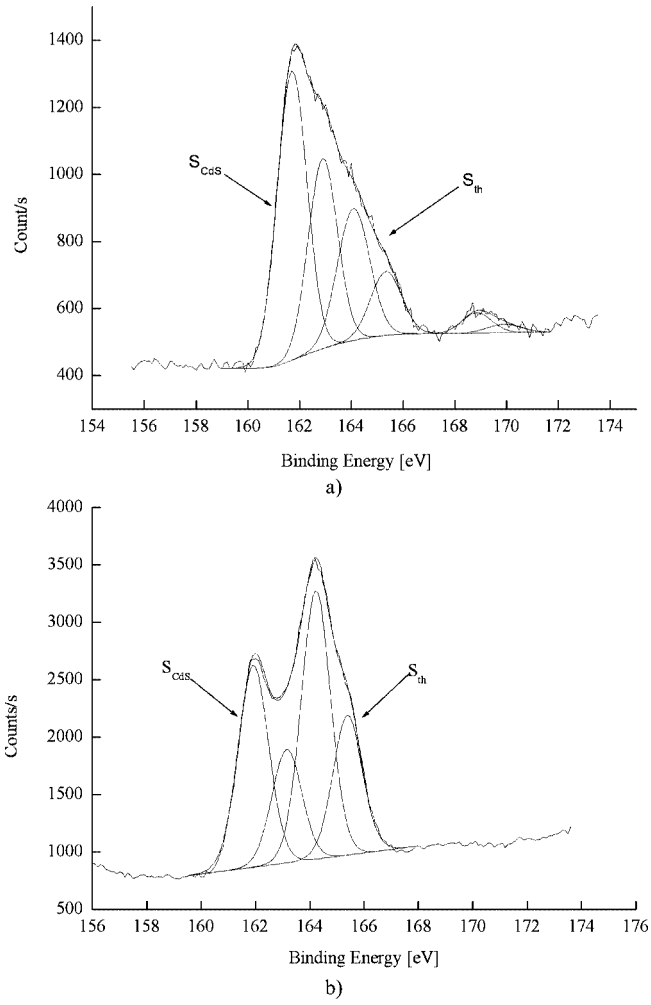

Figure 5. Core level of S2p for **CdS-4T** (top) and **CdS-2T**.

Table 1. Characteristic S2p binding energies (eV) for sulfur within different materials.[a]

Materials	S_{CdS}		S_{Th}		S_{ox}	
	S2p3/2	S2p1/2	S2p3/2	S2p1/2	S2p3/2	S2p1/2
CdS-2T	161.7	162.9	164.1	165.3	168.4	169.9
	40.4	26.3	19.9	9.3	2.83	1.3
CdS-3T	161.6	162.9	164.0	165.2	168.7[b]	
	48.9	25.8	15.4	7.9	1.9	
CdS-4T	161.9	163.2	164.2	165.4	–	–
	28.5	15.7	36.7	19.1	–	–

[a] For each specimen, each sulfur type has an $S2p_{3/2}$-$S2p_{1/2}$ doublet. The binding energy positions are in eV (top line) and the contribution to the total S2p peak area is given in % (bottom line). [b] The S2p peak was very poorly resolved, so $S2p_{3/2}$ and $S2p_{1/2}$ were combined.

Table 2. Apparent surface chemical composition of surface-modified CdS nanoparticles.

Materials	Cd	S_{CdS}	S_T	S_{ox}	C	O	Na
CdS-2T	16.5	10.1	4.39	0.61	49.8	18.6	–
CdS-3T	26.3	16.9	5.19	0.44	36.0	15.2	–
CdS-4T	10.6	7.42	9.33	–	49.4	22.6	0.67

at the CdS and CdSe NC surface. Mulvany et al.[18] and Dushkin et al.[19] reported a version of the hot-matrix method for the synthesis of CdSe nanoparticles using a noncoordinating solvent and a carboxylic acid as the coordinating ligand. This new method is an adaptation of widely reported methods that use cadmium carboxylate salts as precursors for these NCs. Their synthetic approach allows one to tune the nucleation and growth of CdSe by altering the reactivities of selenium and cadmium and to probe more clearly the role of the chalcogenide and cadmium precursors on CdSe nanocrystal synthesis, as well as the role of TOPO on surface passivation. In these systems, it was shown that the usual stabilizing agent, TOPO, can be eliminated completely in favour of a fatty acid without effects on the particle size distribution or their optical properties. They claim that CdSe terminated with a long-chain carboxylate is one of the cleanest colloidal CdSe systems to date, with oleic acid as the sole stabilizer. Peng et al.[20] have developed a successful approach to synthesizing CdS in a noncoordinating solvent. Oleic acid, a natural surfactant, was chosen as the ligand for stabilizing the nanocrystals and the cationic precursors. The ability to use long-chain carboxylic acids as stabilizers was later extended to InP and InAs nanocrystals.[21]

Therefore, it is necessary to estimate the contribution of the carboxylate capping ligands to the total carbon content of the nanoparticles. Figure 6 displays a typical C1s region for **CdS-2T** fitted with five components centred at 285.0, 286.0, 287.4, 288.7 and 290.2 eV. The component centred at 288.7 eV is assigned to the carboxylate group from the oligothiophenes.[22] The contribution of the carboxylate groups to the C1s peak areas of the **CdS-2T**, **CdS-3T** and **CdS-4T** nanoparticles is 11.8, 12.1 and 9.9%, respectively, corresponding to 5.78, 4.35 and 4.88% carboxylate carbon atoms. Note that the contributions of the carboxylates to the C1s region differ slightly from those expected, due to unavoidable adventitious hydrocarbon contamination and the presence of carbonates (peak centred at ca. 290.5 eV).

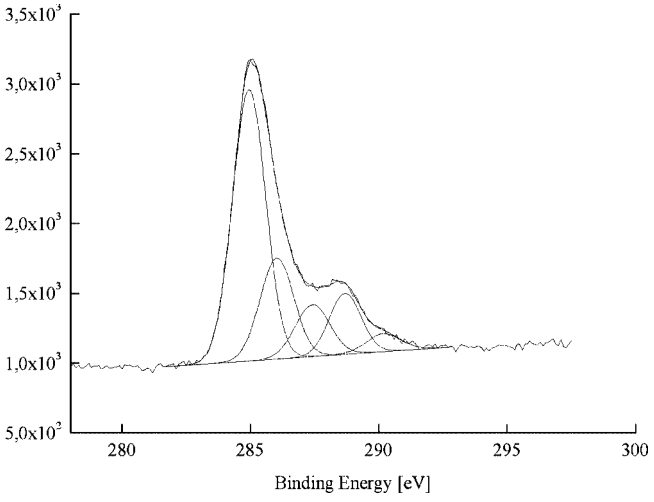

Figure 6. Narrow-scan XPS spectrum of C1s region for **CdS-2T**.

With the contribution of the carboxylates to the surface composition in hand, the $Cd/(S_{CdS}+1/2C_{COO^-})$ atomic ratio, assuming that only one carboxylate group per oligothiophene is coordinated with Cd^{2+} on the particle surface, is 1.26, 1.31 and 1.07, which is in agreement with the stoichiometry of CdS. The contribution of the carboxylates to the surface chemical composition can further be related to the sulfur content due to the oligothiophenes, and the experimental COO^-/S_T molar ratio compared to that expected from microanalysis. Figure 7 shows a plot of the experimental COO^-/S_T molar ratio, as determined by XPS, vs. microanalysis data. The results reflect reasonably well the progressive relative concentration of the carboxylate groups within the oligothiophenes.

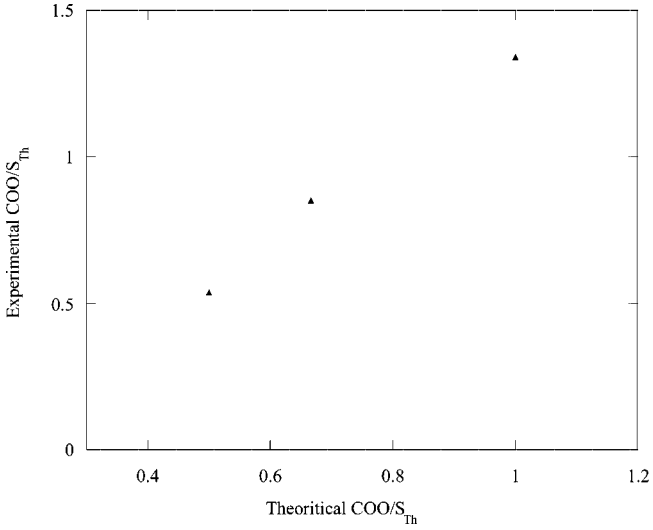

Figure 7. Plot of COO^-/S_T molar ratio, as determined by XPS vs. microanalysis results.

From the surface chemical composition reported in Table 1, one can estimate the number of molecules bound per CdS particle. In this case, only the sulfur of the organic component is considered for the oligothiophenes, and the CdS nanoparticles are, to a first approximation, assumed to be stoichiometric. Because the nanoparticles have also diameters lower than the sampling depth probed by XPS, it is reasonable to assume that the apparent surface composition reflects that of the whole coated nanoparticle. For **Cd-3T** and **CdS-4T** the diameters are estimated to be 3.8 and 2 nm, respectively. Taking into account the density of CdS, and thus the number of Cd atoms per particle, one can estimate the number of bound oligothiophenes per nanoparticle using the ratio $(\%S_T/n_S)/(\%Cd/n_{Cd})$ where $\%S_T$ and %Cd are the atom percents reported in Table 2, n_{Cd} the number of Cd atoms per CdS nanoparticle, and n_S the number of thiophene repeat units per oligothiophene. For **CdS-3T** and **CdS-4T**, we find ca. 19 molecules of terthiophene and 18 molecules of quaterthiophene per nanoparticle.

The hybrid structures of **CdS-*n*T**, with two, three and four rings were characterized by means of absorption and emission spectroscopy. In the UV/Vis studies the structures

were investigated in EG and dimethyl sulfoxide. No marked differences were observed in the absorption spectra of these compounds in either solvent, the resulting spectra being essentially the additive combination of those of the two constituent parts, with slight modification. Figure 8 shows the typical spectra recorded for the CdS–oligothiophene series as well as CdS stabilized by acetate in EG. The NCs stabilized by acetate have an absorption shoulder at 440 nm corresponding to the first excitonic peak. Note that in our studies variation of the synthesis conditions was found to have no significant effect on the excitonic peak energy.

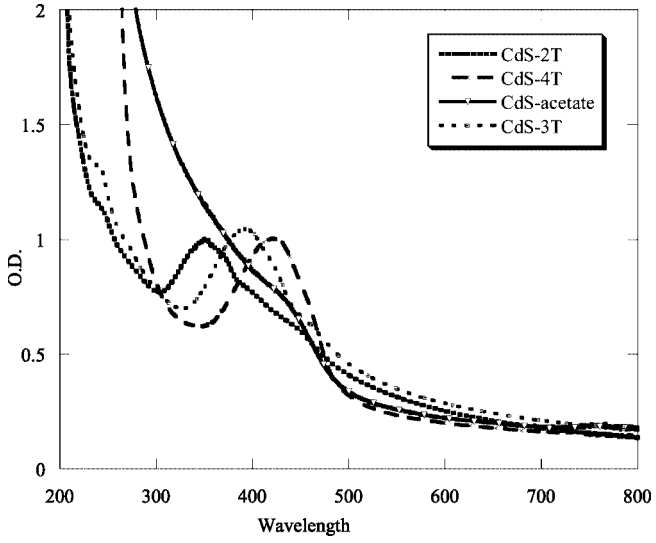

Figure 8. UV/Vis spectra of three samples of **CdS-*n*T** and **CdS-acetate**.

The spectrum of **CdS-*n*T** shows a main peak, in the visible region, due to the π–π* transition, and a weaker but well-defined shoulder at low energy attributed to NC excitonic absorption. The main peak exhibits a perfect correlation with the conjugation length, i.e. the maximum is significantly redshifted as the conjugation length of the corresponding oligothiophene shell increases. Hence, UV/Vis absorption spectra of **CdS-*n*T** show a maximum centred at 350, 395 and 428 nm for **CdS-2T**, **CdS-3T** and **CdS-4T**, respectively. All these maxima were found to be close to those observed for solutions of the oligothiophene dicarboxylates. However, when the spectra of the CdS-bound oligomers are examined carefully the absorption seems not to be a simple superposition of the two components, as can be seen in Figure 9. The easiest case is **CdS-2T**, where the two bands are separate. Additional shoulders appear at the low-energy side of the bithiophene absorption (367 and 400 nm), indicating a ground-state interaction between CdS NCs and the conjugated system. For longer oligomers, the absorption of the organic shell overlaps that of CdS, which makes discussion difficult. The structureless broad absorption observed indicates that the oligomers bound to the nanoparticle surface are relatively flexible for the formation of different conformers in the ground state.

The number of oligomers attached to the nanoparticle is fundamental to fully characterizing the **CdS-*n*T** hybrid core-shell materials. This can be calculated using the absorbance at the oligomer absorption maximum (λ_{max}), that at the CdS excitonic peak (450 nm) and their extinction coefficients. Although the determination of the NC extinction coefficient has been largely debated in the literature, recent work, has established for CdS NCs capped with oleic acid show a strong dependence of the extinction coefficient on the size of the NCs, while the nature of the ligands and the solution refractive index were shown not to have a significant effect.[23] Given the average particle size (4 nm for **CdS-2T**), ε = 552820 L mol^{-1} cm^{-1} for the extinction coefficient of CdS NCs, and 26100 L mol^{-1} cm^{-1} for the extinction co-

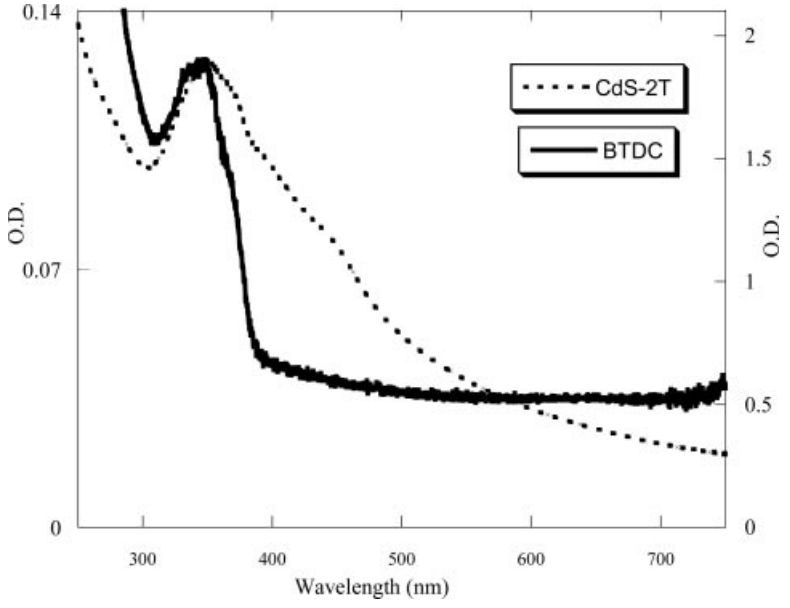

Figure 9. UV/Vis spectra of **CdS-2T** and **BTDC**.

efficient of **BTDC**, the maximum absorbance is 1.88 for **BTDC** and that for the CdS excitonic peak is 1.035. We found that each NC is embedded in 40 **BTDC** molecules. This result is consistent with the work of Milliron et al., who report 50 molecules of pentathiophene per CdSe nanocrystal.[6] Note that the value obtained is relatively low compared to the theoretical one. In fact, 200 molecules were expected to form a close-packed monolayer in a 4-nm diameter sphere. The area occupied per molecule was estimated using the following approximations. The molecule binds perpendicularly to the surface; the area occupied is the projection of the oligomer on the NC. From the known bond lengths, van der Waals atomic radii and the thickness of the oligomers, the area occupied per molecule is estimated to be 24 $Å^2$. Using the same UV/Vis procedure, an average of 18 molecules per NC was found for **CdS-3T**; this value is in good agreement with that estimated from the XPS measurements.

It is well known that the fluorescence properties of CdS NCs depend strongly on their surface states, surface passivation and size distributions. Fluorescence quench or changes in the quantum yield indicate also differences in the branching ratio between radiative and nonradiative decay and therefore might serve as a powerful probe of NC-conjugated polymer interactions. To determine the degree of electronic communication between CdS NCs and oligothiophene, we performed fluorescence measurements. Figure 10 illustrates the room-temperature fluorescence spectra of **CdS-*n*T**. The general trends observed are that the emission of CdS-bound oligothiophenes is weak and exhibits a weak Stokes shift. The intensity drops by a factor of two relative to their homologues, i.e. sodium dicarboxylates. We note also that the emission spectra of **CdS-*n*T** are redshifted relative to the oligothiophenedicarboxylates. This shift is more pronounced for the longer oligomers, i.e. **CdS-3T** and **CdS-4T**. Hence, the emission spectra of **CdS-2T** and its free ligand are similar in energy and shape, except for the low-energy side. **CdS-2T** has a long emission tail in the low-energy part of the spectrum. Quite different emission spectra were obtained for **CdS-3T** and **CdS-4T**, as seen in Figure 10b, c. Those of **TTDC** and **QTDC** sodium salts show two clearly resolved bands at 450 and 465 nm and at 480 and 500 nm, respectively, which have been identified as the vibronic replicas of the O–O transition. These emission maxima are redshifted to 490 and 530 nm for **CdS-3T** and **CdS-4T**, respectively. The intensity of the first band observed for the precursors decreases and becomes a shoulder in **CdS-*n*T**. The similarity in the appearance of the emission spectra of the precursors and CdS-bound oligothiophenes suggests that the origin of this emission is π*–π emission; no CdS NC emission is observed. Selective excitations have been undertaken to analyze the CdS NC emission. Upon excitation into the CdS excitonic absorption band (461 nm), the emission spectrum is similar to that when exciting into the main oligothiophene band, indicating a complete quench of CdS NC fluorescence. The **CdS-*n*T** excitation spectra are similar to the absorption spectra of the oligothiophene precursors.

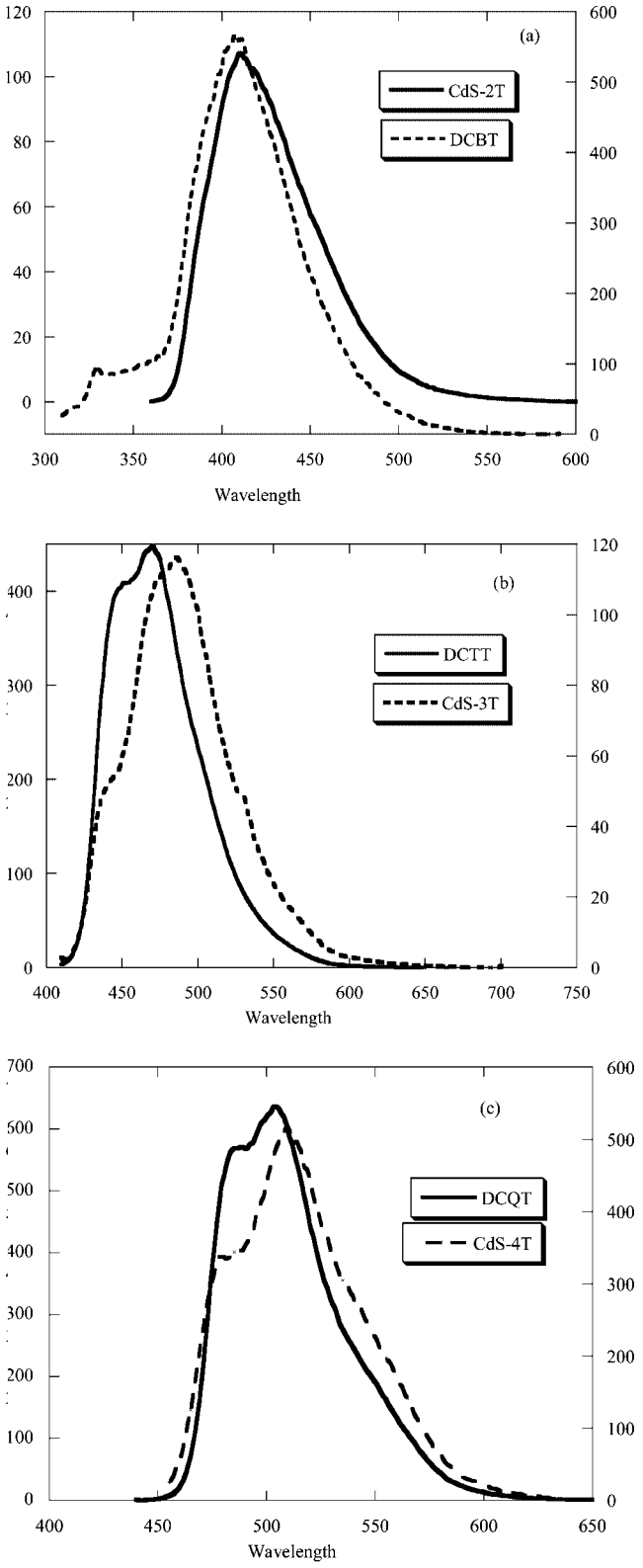

Figure 10. Fluorescence spectra of (a) **CdS-2T** and **BTDC**, (b) **CdS-3T** and **TTDC**, (c) **CdS-4T** and **QTDC**.

The fluorescence changes in the **CdS-*n*T** are in good agreement with the **ZnO-(Th)$_n$** fluorescence observed by Jiu et al. who reported a strong redshift in the precursor emis-

sion, when they were adsorbed on ZnO NC.[24] They found a 100-nm redshift emission of **ZnO-(Th)$_n$** and free precursors. Similar significant modification in the spectral distribution of fluorescence of the CdSe conjugated oligophenylene–vinylene surfactants, relative to blended films of the inorganic and organic components was recently observed by Emrick et al.[3] They attributed this effect to enhanced energy transfer between the conjugated ligand and the quantum dot facilitated by connecting the conjugated backbone directly to the quantum dot.

To help understand the fluorescence results, NC emission properties must be taken into account. Indeed, it has been established that the emission properties of NCs are very sensitive to their surface environment. In general, as-synthesized NCs have high fluorescence quantum yields approaching unity. Decrease in the quantum yield and/or change in the fluorescence shape are considered to be the result of the surface states located in the bandgap of the NCs, which act as trapping states for the photogenerated charges. These surface trapping states originate from the dangling bonds of some of the surface atoms. It has been speculated that in III–V semiconductor NCs, the nanoparticle surfaces are terminated by either cadmium or chalcogen sites. On the other hand, it is well established that an aromatic acid can be bound to a metal surface through the oxygen lone-pair electrons and aromatic carboxylates are also common O-donor ligands in cadmium coordination chemistry. In light of this evidence, and based on published reports showing that carboxylates can act as capping ligands,[18–21] we assume that the oligomer binds to a dangling cadmium ion on the NC surface through the lone-pair electrons of the carboxylate function. In this way, a monolayer of cadmium oligomer complex is formed on the surface of the CdS nanoparticles. This novel supramolecular structure composed of dangling cadmium and conjugated oligomer has more electronic delocalization, which profoundly influences the emission properties of the π-conjugated system of the oligomers. This assumption corroborates well with ab initio calculations made by Puzder et al. The authors calculated the binding energy of different organic functions to a range of the CdSe NC facets.[25] The dominant binding carboxylate interaction found is between oxygen atoms in the ligands and the dangling cadmium atoms on the NC surfaces.

Conclusion

We have prepared a new organic–inorganic structure consisting of oligothiophenes grafted onto the surface of CdS nanocrystals, with narrow size distribution, using a one-pot reaction. The number of bound molecules and the grafting of the oligomers on the surface of the nanocrystals were investigated using XPS, IR, UV/Vis and fluorescence spectroscopy. The bonding of the oligomers to the nanocrystal surface is made possible by complexing the dangling cadmium ion on the surface with the lone-pair electrons of the carboxylate group at the end of the oligomers, leading to better electronic interaction between the two components. On the basis of the observed properties, these hybrid nanoparticles should have potential applications in optoelectronic and photovoltaic devices.

Experimental Section

Materials: All chemicals used in the syntheses and the analytical grade solvents used for UV/Vis studies were purchased from Aldrich and used as received.

Organic Synthesis: 2,2′-Bithiophene-5,5′-dicarboxylic acid (**I**), 2,2′;5′,2″-terthiophene-5,5″-dicarboxylic acid (**II**), and 2,2′;5′,2″;5″,2‴-quaterthiophene-5,5‴-dicarboxylic acid (**III**) were prepared as described in detail elsewhere.[10] All the oligothiophenes were fully characterized by ^{1}H and ^{13}C NMR spectroscopy and elemental analysis.

Synthesis of Oligothiophene-Functionalized CdS Nanoparticles: CdS–oligothiophene hybrid nanoparticles were synthesized in ethylene glycol by the Polyol process.[11] Briefly, the general procedure involves addition of cadmium acetate and thiourea to a given volume of polyol to obtain a concentration between 10^{-2} and 10^{-3} mol L^{-1}. To form CdS–oligothiophene hybrids, oligothiophene with different conjugation lengths was added to the solution. The final oligothiophene concentration was also between 10^{-2} and 10^{-3} mol L^{-1}. The mixture was then heated with vigorous stirring to a temperature varying between 100 and 150 °C. Purification was achieved by adding excess methanol. The precipitate formed was centrifuged and the upper liquid layer decanted, and the isolated solid then dispersed in an appropriate solvent. The above centrifugation and isolation procedure was repeated several times.

General Experimental Procedures: UV/Vis spectroscopy. UV/Vis absorbance spectra were acquired with a Cary 50 spectrometer. Fluorescence spectra were recorded with a Perkin–Elmer LS50 spectrofluorometer. IR spectra were recorded on KBr pellets using a Nicolet IRTF-Magma 860. Transmission electron microscopy (TEM) observations were performed with a JEOL 100 kV JEM-100CX II microscope. The CdS-functionalized nanoparticles were deposited on the amorphous carbon membrane of the transmission electron microscope grid and the solvent then evaporated off at room temperature. The mean diameter was estimated from image analysis of a hundred particles. X-ray powder diffraction (XRD) patterns were recorded with a Philips PW1050/25 using Cu-K_α radiation. The diffractometer was calibrated using a standard Si sample. The counting time was 30 s per 2θ step of 0.05°. The mean crystallite size was estimated using the Scherrer equation. X-ray photoelectron spectroscopy signals were recorded using a Thermo VG Scientific ESCALAB 250 system equipped with a micro-focused, monochromatic Al-K_α X-ray source (1486.6 eV) and a magnetic lens which increases the electron acceptance angle and hence the sensitivity. The specimens were pressed against double-sided adhesive tapes mounted on sample holders, and then pumped overnight in the fast-entry lock at ca. 5×10^{-8} mbar before introduction into the analysis chamber. A 650-μm X-ray beam was used at a power of 13.7 mA × 15 kV. The spectra were acquired in the constant analyzer energy mode, with pass energies of 150 and 40 eV for the survey and the narrow regions, respectively. Charge compensation was achieved with an electron flood gun operated under argon flow at a partial pressure of 2×10^{-8} mbar in the analysis chamber. Under these conditions, the surface charge was negative but perfectly uniform. Avantage software, version 2.2 (Thermo Electron), was used for digital acquisition and data processing.

Spectra were calibrated by setting the C1s peak maximum at 285.0 eV. The apparent surface compositions (in atom%) were determined by considering the integrated peak areas of the C1s, O1s, S2p and $Cd3d_{5/2}$ peaks and the manufacturer's sensitivity factors.

Acknowledgments

The authors wish to thank the Conseil Régional d'Ile-de-France for financial support through the SESAME 2000 Scheme, and Ms. Carole Connan for her assistance with the XPS measurements, Marie-Josèphe Vaulay and Frédéric Herbst for TEM and XRD characterizations.

[1] a) Y. Xia, P. Yang, Y. Sun, Y. Wu, B. Mayer, B. Gates, Y. Yin, F. Kim, H. Yan, *Adv. Mater.* **2003**, *15*, 353–389; b) M. A. El-Sayed, *Acc. Chem. Res.* **2004**, *37*, 326–333.
[2] a) F. Garnier, *Acc. Chem. Res.* **1999**, *32*, 209–215; b) H. E. Katz, Z. Bao, S. L. Gilat, *Acc. Chem. Res.* **2001**, *34*, 359–369.
[3] a) M. Y. Odoi, N. I. Hammer, K. Sill, T. Emrick, M. D. Barnes, *J. Am. Chem. Soc.* **2006**, *128*, 3506–3507; b) H. Skaff, K. Still, T. Emrick, *J. Am. Chem. Soc.* **2004**, *126*, 11322–11325; c) J. Locklin, D. Patton, S. Deng, A. Baba, M. Millan, R. C. Advincula, *Chem. Mater.* **2004**, *16*, 5187–5193.
[4] N. C. Greenham, X. Peng, A. P. Alivisatos, *Phys. Rev. B* **1996**, *54*, 17628–17637.
[5] R. Buller, H. Cohen, E. Minkin, R. Popovitz-Biro, E. Lifshitz, M. Lahav, *Adv. Funct. Mater.* **2002**, *12*, 713–718.
[6] D. J. Miliron, A. P. Alivisatos, C. Pitois, C. Edder, J. M. J. Fréchet, *Adv. Mater.* **2003**, *15*, 58–61.
[7] B. Sun, E. Marx, N. C. Greenham, *Nano Lett.* **2003**, *3*, 961–963.
[8] W. J. E. Beek, R. A. J. Janssen, *Adv. Funct. Mater.* **2002**, *12*, 519–525.
[9] J. Liu, T. Tanaka, K. Sivula, A. P. Alivisatos, J. M. J. Frechet, *J. Am. Chem. Soc.* **2004**, *126*, 6550–6551.
[10] J. Kagan, S. K. Arora, A. Usunol, *J. Org. Chem.* **1983**, *48*, 4076–4078.
[11] a) G. Viau, R. Brayner, L. Poul, N. Chakroune, E. Lacaze, F. Fiévet-Vincent, F. Fiévet, *Chem. Mater.* **2003**, *15*, 486–494; b) C. Feldmann, Ch. Metzmacher, *J. Mater. Chem.* **2001**, *11*, 2603–2606.
[12] T. Matrab, A. Yassar, G. Viau, N. Chakroune, F. Fievet, P. C. Lacaze, *J. Colloid Interface Sci.* **2006**, *296*, 95–101.
[13] B. Simmons, S. Li, V. T. John, G. L. McPherson, A. Bose, W. Zhou, J. He, *Nano Lett.* **2002**, *2*, 263–268.
[14] M. J. Byrnes, M. H. Chisholm, R. J. H. Clark, J. C. Gallucci, C. M. Hadad, N. J. Patmore, *Inorg. Chem.* **2004**, *43*, 6334–6344.
[15] R. C. Mehrotra, R. Bohra, *Metal Carboxylate*, Academic Press, New York, **1983**.
[16] a) U. Winkler, D. Eich, Z. H. Chen, R. Fink, S. K. Kulkarni, E. Umbach, *Phys. Stat. Sol. A* **1999**, *173*, 253–259; b) J. E. Bowen Katari, V. L. Colvin, A. P. Alivisatos, *J. Phys. Chem.* **1994**, *98*, 4109–4117.
[17] a) H. Encai, S. Haiping, Z. Zheng, L. Junqiu, Y. Bai, S. Jiacong, *Chem. Mater.* **1999**, *11*, 3096–3102; b) B. Schreder, T. Schmidt, V. Ptatschek, U. Winkler, A. Materny, E. Umbach, M. Lerch, G. Müller, W. Kiefer, L. Spanhel, *J. Phys. Chem. B* **2000**, *104*, 1677–1685.
[18] A. Jasieniak, C. Bullen, J. Embden, P. Mulvaney, *J. Phys. Chem. B* **2005**, *109*, 20665–20668.
[19] G. G. Yordanov, G. D. Gicheva, B. H. Bochev, C. D. Dushkin, E. Adachi, *Colloids Surf. A* **2006**, *273*, 10–15.
[20] W. W. Yu, X. Peng, *Angew. Chem. Int. Ed.* **2002**, *41*, 2368–2371.
[21] D. Battaglia, X. Peng, *Nano Lett.* **2002**, *2*, 1027–1030.
[22] http://srdata.nist.gov/xps
[23] W. W. Yu, L. Qu, W. Guo, X. Peng, *Chem. Mater.* **2003**, *15*, 2854–2860.
[24] T. Jiu, H. Liu, H. Gan, Y. Li, S. Xiao, H. Li, Y. Liu, F. Lu, L. Jiang, D. Zhu, *Synth. Met.* **2005**, *148*, 313–319.
[25] A. Puzder, A. J. Williamson, N. Zaitseva, G. Galli, L. Manna, A. P. Alivisatos, *Nano Lett.* **2004**, *4*, 2361–2361.

Received: July 7, 2006
Published Online: February 9, 2007

